PHYSICAL REVIEW B **79**, 205423 (2009)

Surface phonon dispersion curves of thin Pb films on Cu(111)

Jens Braun,* Paolo Ruggerone,† Ge Zhang,‡ and J. Peter Toennies§
Max-Planck-Institut für Dynamik und Selbstorganisation, Bunsenstraße 10, 37073 Göttingen, Germany

Giorgio Benedek
Dipartimento di Scienza dei Materiali, Universitá di Milano-Bicocca, Via R. Cozzi 53, 20125 Milano, Italy and Donostia International Physics Centre (DIPC), 20018 Donostia/San Sebastian, Spain

(Received 19 December 2008; published 22 May 2009)

Thin films of lead have been grown on the Cu(111) surface and their structure and phonon dispersion curves have been investigated with high-resolution helium atom scattering. The diffraction pattern of the first monolayer (ML) indicates a $p(4\times4)$ structure. Films consisting of $N=3$, 4, 5, and bulklike 50 ML all have a regular (1×1) structure with the same lattice constant as the bulk and small superimposed $p(4\times4)$ peaks for the thinnest films. The time-of-flight spectra reveal an unusually large number of inelastic peaks for all the films. The results have been analyzed in terms of dispersion curves which exhibit more than $\frac{1}{2}$ the total number of expected two N modes active in the planar scattering geometry. Dispersion curves for an unannealed 5 ML film are also reported. A force-constant model fitted to the bulk dispersion curves can only qualitatively reproduce some of the data but help to explain some features. Along the $\bar{\Gamma}-\bar{K}$ direction, a Kohn anomaly is identified for the 3, 4, and 5 ML films at nearly the same wave vector as in the bulk along the equivalent direction.

DOI: 10.1103/PhysRevB.79.205423 PACS number(s): 68.35.Ja, 68.47.−b, 68.65.Fg, 68.55.at

I. INTRODUCTION

Although lead is classified as a simple metal, it has many unique and unusual physical properties. Many of these result from its large electron-phonon coupling constant $\lambda=1.53$, which is one order of magnitude larger than in the noble metals.[1] As a consequence it has—among the elements—a comparatively high superconducting critical temperature of 7.23 K. The bulk phonon dispersion curves of lead crystals are characterized by several Kohn anomalies, which were the first to be detected.[2] Kohn anomalies require exceptionally long-ranged interatomic force constants extending to distances up to 20 Å in order to be reproduced within a pure Born–von Kármán scheme. Thus even a 26-parameter force-constant model was found to be inadequate to fit the data.[3] So far most theoretical attempts to fit and explain the anomalies in the bulk dispersion curves have not been entirely successful.[4] The density-functional calculations by de Gironcoli,[5] Savrasov and Savrasov,[6] and Grabowski *et al.*[7] as well as the linear-response calculations of Liu and Quong[8] reproduce some of the Kohn anomalies but are not successful in fitting the phonon frequencies in all regions of k space. The best agreement also with respect to the Kohn anomalies has very recently been achieved by Dal Corso,[9] who carried out a fully relativistic density-functional calculation which includes the spin-orbit coupling.

Other manifestations of a large electron-phonon coupling are the quantum-size effects (QSEs), which were first found in thin lead metal films.[10] Now with the advances in ultrahigh-vacuum (UHV) film technology, a wide variety of different quantum-size phenomena have been observed in lead films consisting of $N=1$ to 50 well-defined layers. Film properties affected by a QSE include the photoemission spectra,[11] the Hall coefficient,[12] the superconducting transition temperature,[13] and the work function.[14] The QSEs are so strong that they even affect the kinetics of layer growth to the extent that the double-layer growth predominates over layer-by-layer growth[10] and also affects the effective layer heights[15] as well as the preferred heights of nanoislands.[16] These many phenomena have stimulated a large number of theoretical investigations of surface energies and work functions,[17–24] surface states,[20,21] charge densities and relaxation,[18,22] and very recently the surface phonons at the Brillouin-zone center.[24]

At present there is virtually no information on the extent to which a QSE affects film properties parallel to the surface.[24] At first sight, such an effect might not be expected since the many quantum-size effects described above all are related to the quantum well states (QWSs) normal to the surface. With an increasing layer thickness each time an additional QWS falls below the Fermi energy, however, the surface work functions,[14] the electron spillout,[25] and the surface energies[17,18] are all affected. Thus it is, in fact, quite reasonable to expect that the interatomic forces between the atoms at the surface might also undergo changes. Especially when it is recalled that numerous helium atom scattering (HAS) studies of surface phonons have demonstrated that due to the reduced coordination at the vacuum interface, the electron-phonon interaction is stronger at the surface than in the bulk, especially in metals.[26,27] Thus the aim of the HAS surface phonon experiments described here was to search for the influence of the electron confinement on the phonons of thin lead films. Having two closely spaced interfaces, the phonons of thin films should also provide an especially discriminatory test of theories of atomic forces in metals. In addition, this study was motivated by a search for Kohn anomalies, which are known to be strongly enhanced in two dimensional systems.[28]

In the past, Kohn anomalies have only been observed in the surface phonon dispersion curves of a few metals, namely, Pt(111),[29] H/W(110),[30] and H/Mo(110).[31] On Pt(111), only small discontinuities in the slope (group veloci-

ties) of the Rayleigh mode dispersion curve are observed. On the W(110): H(1×1) and Mo(110): H(1×1) surfaces; however, a deep sharp minimum is found with HAS, which is less distinct in related electron-energy-loss spectroscopy (EELS) experiments.[32] Kohn anomalies also show up as large dips in the dispersion curves of layered compounds, such as 2H-$TaSe_2$,[33] where the effect is clearly related to the 2D nature of these crystals.

The few measurements of surface phonon dispersion curves for thin metal films with three or more layers have been mainly for the alkali atoms Na, K, and Cs on Cu(001), on Cu(111) and Ni(001) substrates,[34–36] as well as on graphite.[37] In most cases, the observed dispersion curves were attributed to film vibrations perpendicular to the surface called organ-pipe modes, which are the phonon analog of the electronic quantum well states.[35] Kohn anomalies could so far not be identified in any of these thin-film studies.

The present paper is organized as follows. Section II describes the important details of the HAS apparatus and how the films were grown. The He atom diffraction patterns measured for films of different thickness indicate a regular (111) structure for films with three or more layers. Some of the several hundred measured time-of-flight (TOF) spectra are presented as transformed energy-transfer spectra. The intensities as a function of wave-vector transfer are used to establish the polarizabilities of some of the modes along $\bar{\Gamma}\bar{K}$. The dispersion curves measured along the $\bar{\Gamma}\bar{M}$ and $\bar{\Gamma}\bar{K}$ directions for thin 3, 4, and 5 ML films and for a thick 50 ML film with a bulklike surface are then presented and compared to bring out the changes which appear upon addition of another film layer. The surface phonon dispersion curves reported here exhibit a much richer structure than all previous thin-film studies. Moreover, the number of dispersion curves is unusually large and increases with the layer thickness. More than half of the maximum $2N$ vertically and longitudinally (sagittal plane) polarized phonon dispersion curves, which can be excited, were observed for films with $N=3$, 4, 5, and 50 ML. The effect of annealing on the $\bar{\Gamma}\bar{K}$ dispersion curves 3 of a 5 ML film is also presented. In Sec. IV the results are compared with calculations based on a new Born–von Kármán fit of the bulk phonon dispersions curves. Some of the important differences between the theory and experiment are analyzed. Several shortcomings of the calculations and their influence on the results are assessed in the summary (Sec. V). Finally, it is pointed out that the present investigation complements earlier HAS measurements of the surface phonon dispersion curves of monolayer lead films on Cu(111) and of a 20% Tl stabilized bilayer lead film, which without the addition of Tl would be unstable.[38]

II. APPARATUS

The measurements were carried out on two high-resolution inelastic helium atom scattering (IHAS) apparatus: HUGO I described in Ref. 39 and GURKE described in Ref. 40. Briefly both consist of a high-pressure free jet beam source, which produces an intense beam of He atoms with kinetic energies between $E=10$ meV($k=4.4$ Å^{-1}) and 97 meV($k=13.6$ Å^{-1}) at source temperatures of $T_0=45$ K and $T_0=450$ K, respectively. These atom beams have a relative velocity half width of 1%[41] facilitating high-resolution TOF measurements of the rotating-disc-chopped beam with a pulse width of about 10 μs. The overall flight distance of about 120 cm in both apparatus corresponds to flight times of 2×10^{-3} and 6×10^{-4} s, respectively, for the energies listed above. Since the angle between the incident and scattered beam is fixed at $\theta_{SD}=90°$, the wave-vector transfers are given by $\Delta K=k_i \sin\theta_i - k_f \sin(90-\theta_i)$. A wide range of wave-vector transfers is easily accessed by simply rotating the crystal about an axis, which intersects the two beams, and is perpendicular to the plane of the two beams. The target is housed in an ultrahigh-vacuum sample chamber ($p\leq 5\times10^{-11}$ bar) equipped with low-energy electron diffraction (LEED) and Auger for initial sample preparation and characterization during the measurements. The lead layers were deposited via an effusive beam from a radiation-heated Knudsen cell situated in the sample chamber 5 cm from the target. The target temperature during deposition was about 140 K. In both sets of experiments, the freshly prepared films were then annealed either at 270 K (experiment A) or at 250 K (experiment B) for about 15 min in order to remove the strain in the freshly deposited layers.[42,43] At these annealing temperatures, the alloying observed to take place at step edges at temperatures slightly above room temperature[44] is not expected. The final characterization of the substrate surface, the newly prepared film surface, as well as the layer thickness were provided by HAS drift spectra,[45] diffraction patterns, and specular peak intensity oscillations during growth.[10,46] The substrate and film surfaces were of the same good quality as other surfaces prepared in our laboratory with a surface coherence length of several tens of nanometers.

A typical set of time-of-flight measurements for one film took typically several hours and no signal degradation was observed after more than 20 h. The first series of measurements was carried out for $N=3-7$ and $N=50$ by Zhang[47] on HUGO I (experiment A) and later repeated with an improved signal-to-noise ratio for $N=3-6$ and $N=50$ by Braun and Toennies[25] on the GURKE apparatus (experiment B) with nearly identical results.

III. EXPERIMENTAL RESULTS

A. Diffraction patterns

As mentioned above and described in detail in Ref. 10, the film deposition was monitored by measuring the specular intensity during growth and counting the maxima which indicate the completion of an additional layer. Figure 1 shows a series of angular distributions starting with the clean Cu(111) surface [Fig. 1(a)] upon which films with 1, 3, and 5 ML and a thick film with 50 ML had been deposited and annealed. The Cu(111) surface exhibits only very weak first-order diffraction peaks along the $[1\bar{2}1]$ azimuth which are a factor of $\approx 2\times10^{-4}$ smaller than the specular peak. In the $[1\bar{1}0]$ azimuth, there is no evidence for first-order peaks and their intensity relative to the specular peak is less than ≈ 2

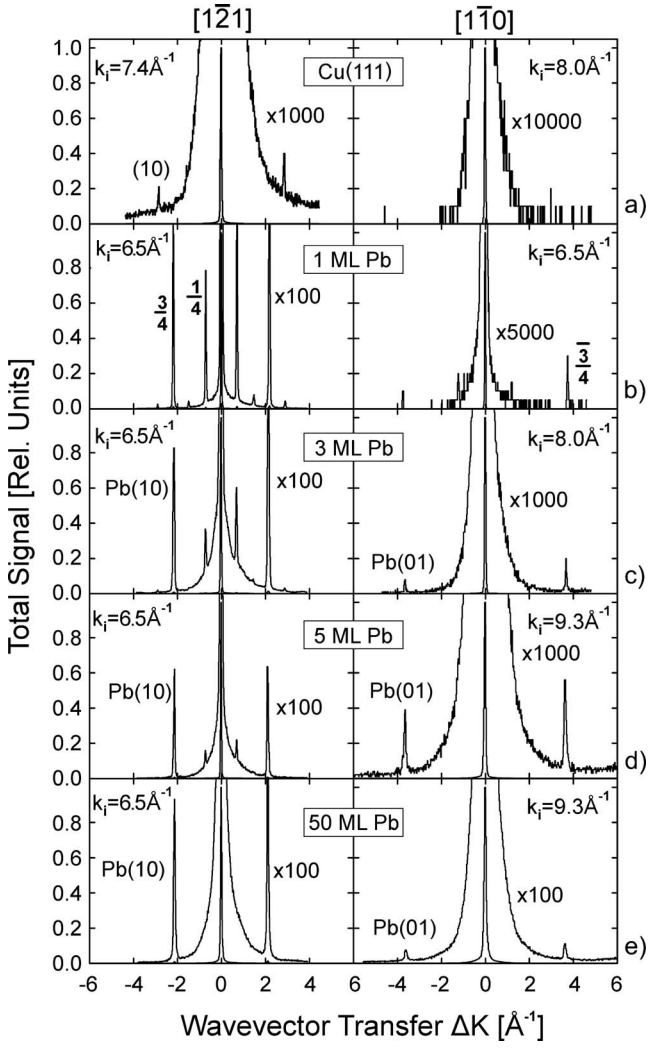

FIG. 1. HAS angular distributions (experiment B) for the (a) clean Cu(111) substrate, (b) 1 ML lead, (c) 3 ML lead, (d) 5 ML lead, (e) and a thick 50 ML lead film. The peaks seen along the $[1\bar{2}1]$ direction at 1 ML are due to the compressed $p(4\times4)$ structure (Ref. 38) which still has a weak influence on the 3 and 5 ML diffraction patterns. The relatively large diffraction peak intensities of the lead layers correspond to a hard-sphere corrugation amplitude of about 1.2×10^{-3} nm (Ref. 50).

$\times10^{-5}$. These observations are consistent with a very smooth surface with a corrugation amplitude of less than 2×10^{-4} nm which is less than that found for most other (111) noble-metal surfaces.[48,49] The diffraction pattern [Fig. 1(b)] for a 1 ML lead film is consistent with a $p(4\times4)$ structure as reported earlier with HAS (Ref. 38) and LEED.[43] Results are not available for 2 ML since, as observed earlier, a 2 ML film is not stable and the first fully occupied smooth layer consists of 3 ML.[10] Although greatly reduced in intensity, the same $p(4\times4)$ diffraction peaks are still seen at 3, 4, and 5 ML indicating that the corrugation of the monolayer structure is still embossed on the outer layers. The diffraction patterns and intensities of all the lead films exhibit sharp intense first-order peaks indicating a (111) surface structure with an estimated hard-sphere surface corrugation amplitude of about 1.2×10^{-3} nm along the $[1\bar{2}1]$ azimuth.[50] All films

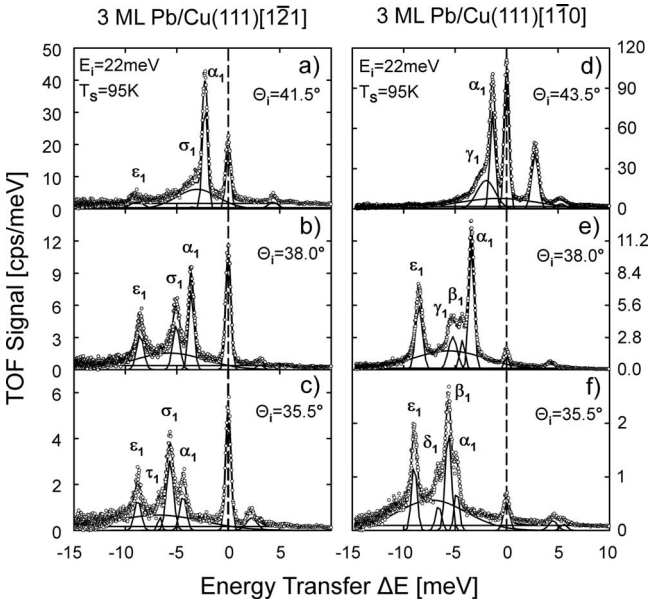

FIG. 2. Some representative inelastic He atom energy-transfer spectra (experiment B) measured for 3 ML Pb/Cu(111) along the two symmetry directions with a beam energy of 22 meV (k_i=6.5 Å^{-1}) and a surface temperature of T_s=95 K. The underlying smooth curves show constituent Gaussian peaks and a broad multiphoton background which were fitted to the spectra to identify the contributions from the individual dispersion curves. The Greek letters indicate modes belonging to a specific dispersion curve.

with $N\geq3$ ML have a lattice constant which is to within better than 1% equal to the bulk lattice constant a=4.95 Å. The small lateral compression of up to 3.3% observed previously[43] for LEED with increasing layer thickness from 1.0 to 1.2 ML at 180 K was not observed although the HAS resolution was sufficient. The diffraction peak positions of the thick 50 ML layer are also consistent with the structure of the ideal Pb(111) surface.

B. Energy-transfer spectra from time-of-flight measurements

Figure 2 shows some typical energy-transfer spectra obtained by transforming the measured time-of-flight spectra[51] for a 3 ML annealed surface. In order to identify the contributions of individual modes to the dispersion curves, the spectra were least squares fitted by a series of sharp Gaussian peaks as well as an underlying broad Gaussian distribution to account for the multiphonon background. In these and other TOF spectra at small incident scattering angles Θ_1, which sample the largest range of phonon energies, four of the expected total of $3\times2=6$ sagittal plane modes can be identified. Such a relatively large fraction of the total possible number of modes has not been seen previously in any of the studies of metal films nor on the surfaces of bulk metal crystals.

Figure 3 presents a series of energy-transfer spectra for 3, 4, and 5 ML Pb at nearly the same scattering angles of 41.5° and 38.5° along the $[1\bar{2}1]$ and $[1\bar{1}0]$ azimuths, respectively. The energy-transfer spectra for 3, 4, and 5 ML Pb shown in Fig. 3 illustrate the appearance and disappearance of some

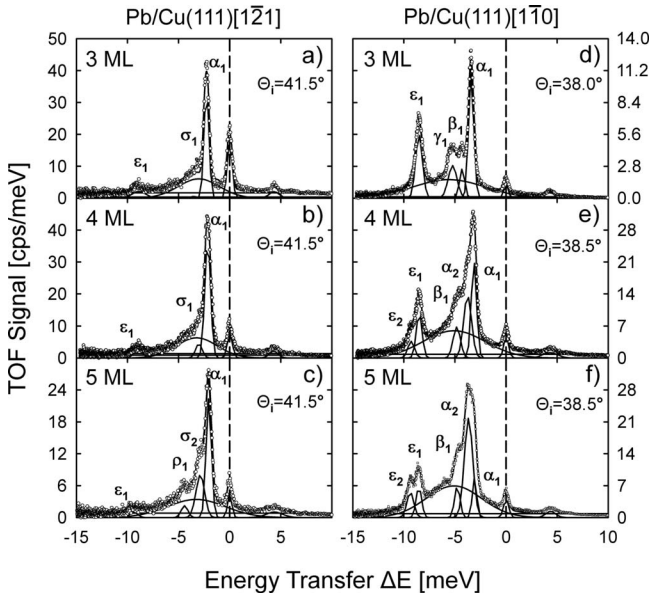

FIG. 3. Comparison of energy-transfer spectra for three different coverages 3, 4, and 5 ML along the $\bar{\Gamma}\bar{M}[1\bar{2}1]$ and $\bar{\Gamma}\bar{K}[1\bar{1}0]$ azimuths for identical incident-beam energies of 22 meV (k_i =6.5 Å^{-1}), surface temperatures T_s=95 K, and similar incident scattering angles Θ_1=41.5°($\bar{\Gamma}\bar{M}$) and Θ_1=38.5($\bar{\Gamma}\bar{K}$) (experiment B).

modes and the overall proliferation in the number of sagittal modes with layer thickness. For those modes, which are common to all three layers, only small but significant energy differences are seen with increasing layer thickness.

Figure 4 provides a further comparison of the energy-transfer spectra for 3, 4, 5, and 50 ML films at four different angles along the $[1\bar{1}0]$ direction. The comparison reveals the complicated evolution of the intensities and appearance and disappearance of peaks with decreasing scattering angles which correspond to an increase in energy and wave-vector transfer. Whereas at small wave-vector transfer the α_1 and α_2 peaks dominate the spectra, they disappear at larger wave-vector transfer and are replaced by the β_1 and β_2 peaks. Especially in the 3 ML film, the large energy-transfer region is dominated by the ε_1 and to a lesser extent by the ε_2 peaks.

The energies of the individual inelastic peaks are affected by a number of intrinsic factors,[51] such as the angle with which the scan curve crosses the dispersion curves (e.g., Fig. 6), as well as by extrinsic factors such as the velocity spread of the incident beam and the TOF resolution.[52] The overall errors can be estimated from the half widths of the best fit Gaussian peaks in Figs. 2–4, where they vary between 0.5 and 1.3 meV. The relative errors from point to point along a given dispersion curve will generally be much smaller and less than about 0.2–0.3 meV. The corresponding errors in wave vector are less than about 0.04 Å^{-1}.

C. Inelastic peak intensities

The dependence of the inelastic peak intensities on the wave-vector transfer provides information on the polarization of the various modes. Figure 5 shows a series of measurements of the inelastic peak intensities as a function of the wave-vector transfer for the α_1, α_2, β_1, ε_1, and ε_2 modes along the $\bar{\Gamma}\bar{K}$ direction for 3, 4, and 5 ML annealed films. The nearly exponential falloff of the α and ε modes indicates that these are largely shear-vertical (SV) polarized.[53,54] The

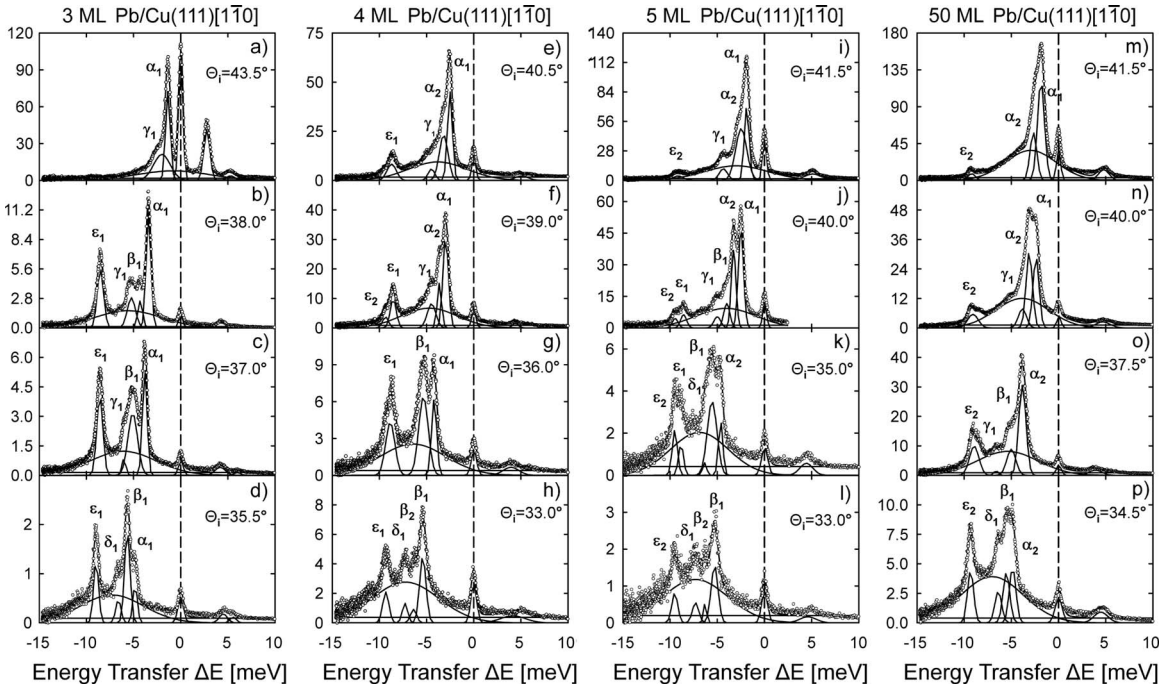

FIG. 4. Comparison of energy-transfer spectra (experiment B) for four different coverages 3, 4, 5, and 50 ML along the $\bar{\Gamma}\bar{K}$ [$1\bar{1}0$] azimuth at four different angles under otherwise identical conditions of incident-beam energies of 22 meV (k_i=6.5 Å^{-1}) and surface temperatures T_s=95 K.

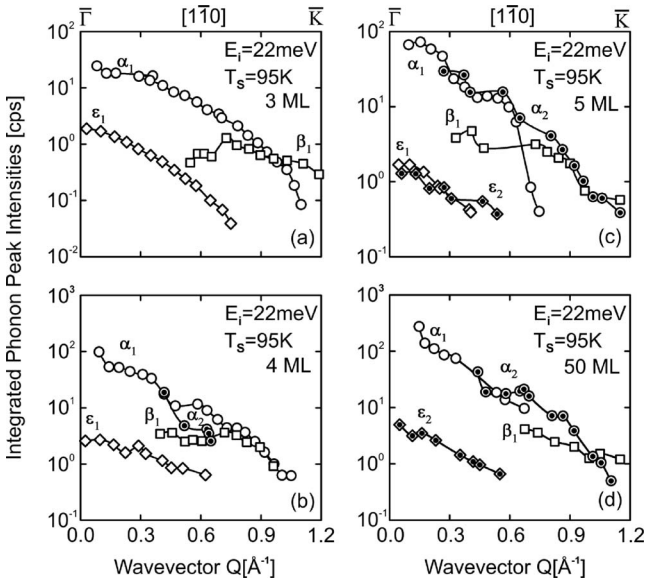

FIG. 5. The areas under the inelastic energy-transfer peaks α_1, α_2, β_1, ε_1, and ε_2 (see Figs. 6–9) are plotted as a function of the surface wave-vector transfer for the 3, 4, and 5 ML films and 50 ML bulk-like surface. The incident-beam energies are 22 meV (k_i=6.5 Å^{-1}) and the surface temperatures T_s=95 K.

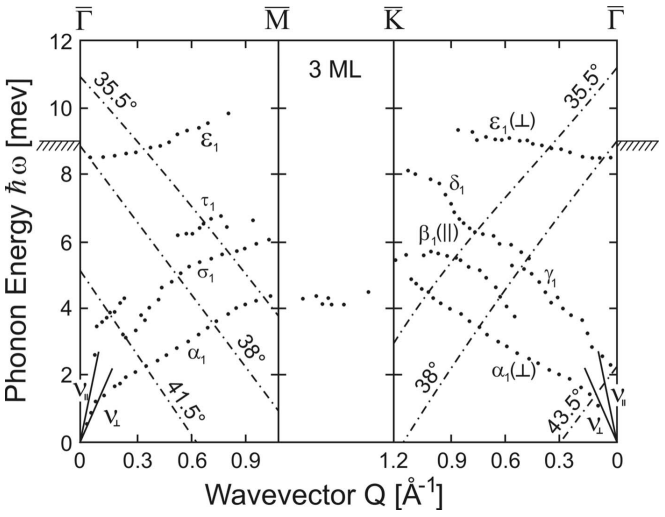

FIG. 6. Surface phonon dispersion curves for 3 ML lead (annealed) on Cu(111) measured with E_i=22 meV and T_s=95 K. The dotted-dashed diagonal continuous lines are the scan curves corresponding to the measurements in Fig. 2. The diagonal straight lines starting at $\bar{\Gamma}$ are the velocities of the substrate Rayleigh mode ($\nu_\perp$) and of the longitudinal band edge ($\nu_\parallel$) projected onto the surface. The maximum bulk phonon frequency of 9.04 meV is indicated by the striped band edge at both sides.

β_1 modes exhibit a different more complicated behavior with wave-vector transfer. Their more gradual falloff at wave-vector transfers up to about 0.8 Å^{-1} in the 3, 4, and 5 ML films suggests a behavior expected for a longitudinally polarized mode.[53,54] In the 4 and 5 ML modes, the β modes undergo a transition to a significantly greater exponential slope, which is the same as the α_1 mode. This suggests a hybridization, presumably resulting from a crossing with another shear-vertical polarized mode at larger wave-vector transfers. Unfortunately, the other mode causing the hybridization cannot be clearly identified in the dispersion curves in Figs. 7 and 8.

D. Experimental dispersion curves

1. Dispersion curves for 3 ML

Figure 6 presents the measured values of energy transfer $\hbar\omega$ and wave-vector transfer Q (=ΔK) in a reduced zone representation for a 3 ML lead film. The presented dispersion curves are from a critical analysis of the data of both experiments A and B. In the few cases, where differences appeared, preference was given to the more recent experiment B data. The dash-dotted curves show some representative scan curves, which correspond to the energy-transfer spectra in Fig. 2. Altogether four or possibly five modes are clearly found along the $\bar{\Gamma}\bar{M}$ and also along the $\bar{\Gamma}\bar{K}$ azimuth. As mentioned earlier, the observation of so many modes is quite unusual. In nearly all of the previous thin-film studies, only about two modes were observed. Three of the $3N$=9 total number of possible modes must be predominantly vertically polarized. At the zone center, they correspond to the *organ-pipe modes* originally observed in Na films[34] and are expected to couple strongly to He atoms. Thus of the four or five observed modes, the remaining one or two modes must be longitudinally polarized. The other three of the nine possible modes are shear horizontally (SH) polarized and their excitation is forbidden along high-symmetry directions.

The dispersion curves in both directions show an irregular seemingly erratic behavior. Some of this unusual behavior near the $\bar{\Gamma}$ point may be influenced by the Rayleigh and longitudinal modes of the underlying Cu(111) substrate with velocities $\nu_\perp$ and $\upsilon_\parallel$, respectively, as indicated by the straight lines for both directions in Fig. 3. Thus the initial steep slope seen at small wave vectors along $\bar{\Gamma}\bar{M}$ followed by the sharp kink and leveling off with increasing wave vector may be caused by the long-wavelength Rayleigh modes of the substrate, which are transmitted through the film. A backward extrapolation to the $\bar{\Gamma}$ point of the data beyond the kink suggests that the lowest-energy mode may have a gap at $\bar{\Gamma}$. The behavior of the highest-energy optical mode ε_1 is also surprising since with increasing wave vector its energy rises above the maximum of the bulk phonon energies at 9.037 meV[2]. Possible explanations for the apparently too large frequencies which are also seen for all the annealed films as well as the bulk surface will be postponed until the end of Sec. III D 2.

2. Dispersion curves for 4, 5, and 50 ML

Figure 7 shows the measurements for a 4 ML film and compares the experimental points with smooth curves fitted to the data points in Fig. 4 for a 3 ML film in order to bring out the differences. Along $\bar{\Gamma}\bar{M}$ at least four and possibly even five modes are clearly observed, which differ only slightly from the corresponding 3 ML curves. The appearance of a

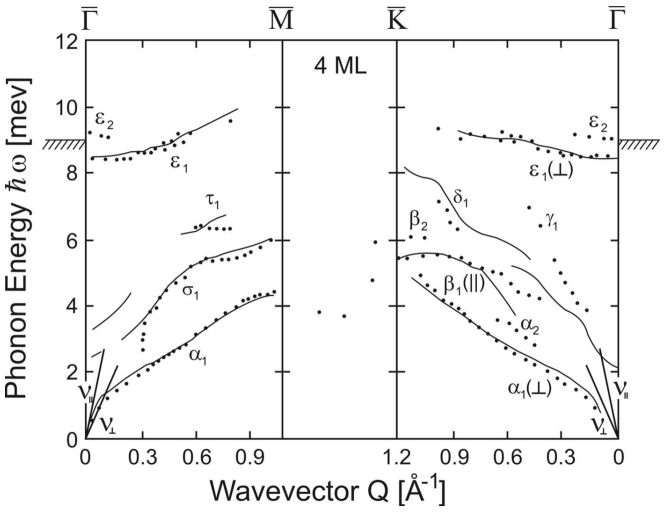

FIG. 7. Same as Fig. 6 but for 4 ML. The continuous lines are smoothed curves drawn through the experimental points for 3 ML plotted in Fig. 6.

second optical mode ε_2 near $\bar{\Gamma}$ is unusual since it lies slightly above the bulk phonon maximum energy even at the zone origin. Thus it cannot propagate inside the film and must be localized at the surface. In this respect, the mode ε_2 is not a true organ-pipe mode.[34,55]

More dramatic differences are seen in the $\bar{\Gamma}\bar{K}$ direction (Fig. 7) where at least seven modes can be identified, several of which are not found in the 3 ML film. The other modes are significantly shifted with respect to the 3 ML modes. The new optical mode ε_2 with the highest energy is the continuation of the same mode mentioned above observed along $\bar{\Gamma}\bar{M}$.

Figure 8 presents the data for 5 ML and for comparison smoothed curves through the data measured for 4 ML. In this case, the incremental differences in the dispersion curves are smaller than for the increment from 3 to 4 ML as might be

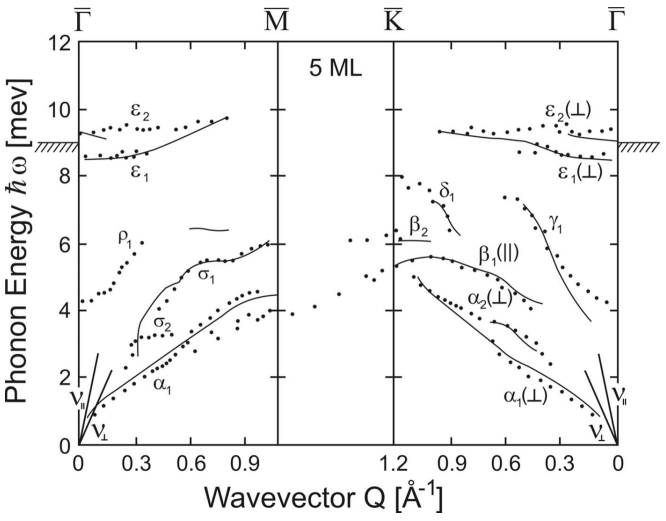

FIG. 8. Same as Fig. 6 but for 5 ML. The continuous lines are smoothed curves drawn through the experimental points for 4 ML plotted in Fig. 7.

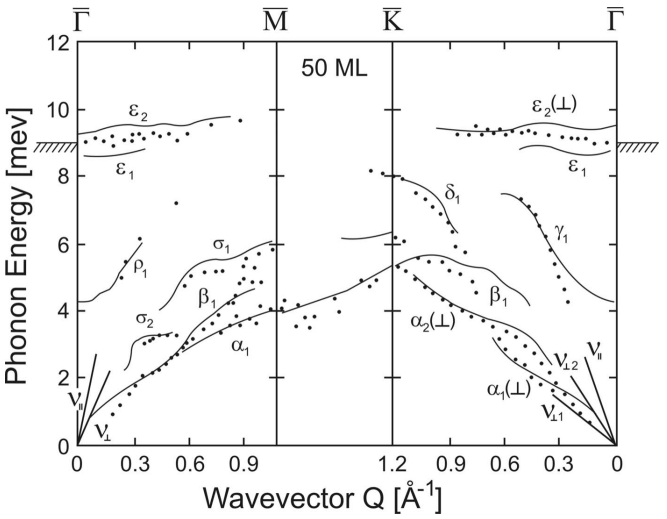

FIG. 9. Same as Fig. 6 but for 50 ML, which is equivalent to a semi-infinite crystal. The continuous lines are smoothed curves drawn through the experimental points for 5 ML plotted in Fig. 8. The diagonal straight lines starting at Γ along $\bar{\Gamma}\bar{K}$ show the bulk lead surface velocities of the transverse $(\nu_{\perp 1}, \nu_{\perp 2})$ and the longitudinal $(\nu_{\|})$ surface modes.

expected because of the smaller fractional relative increase. Along $\bar{\Gamma}\bar{M}$ at least six and probably seven distinct modes are seen. The lowest-energy mode α_1 appears to be split into two modes at about half way out to the zone boundary. Also a new optical mode ρ_1 is seen starting at about 4 meV at $\bar{\Gamma}$, which was not seen for 4 ML. The highest-energy optical mode ε_2 now extends out to larger wave vectors.

Figure 9 shows measurements for a 50 ML film in comparison with smoothed lines drawn through the 5 ML data. Even thicker films up to 300 ML (experiment A) showed no significant differences so that the 50 ML surface phonons are essentially those of the bulk surface. The advantage over measurements on a bulk sample is the greater purity and ease of production of the evaporated layers. The splitting of the lowest mode along the $\bar{\Gamma}\bar{K}$ direction is reminiscent of a similar behavior found in Au(111) along the same direction.[56] In this direction, the sagittal plane has no mirror symmetry and none of the modes has an exact SH polarization.[57] Thus also the quasi-SH modes may acquire a small amplitude and appear in the sagittal planar TOF spectra. This interpretation is however incompatible with the fact that the α_1 and α_2 HAS peaks have comparable intensities (Figs. 4 and 5). More likely, the modes α_1 and α_2 are both quasisagittal $(\perp)$ modes.

The biggest difference compared to the 5 ML film dispersion curves is the disappearance of the ε_1 mode. This suggests that unlike ε_2, the ε_1 mode can be assigned to an organ-pipe mode whose surface amplitude is only appreciable for films of small thickness. On the other hand, the persistence of the ε_2 above the bulk maximum frequency (9.037 meV) also at 50 ML suggests for this anomaly a mechanism common to films of any thickness. It cannot be related to the large electron spillout of the valence electrons seen in our earlier HAS study[15] and nicely reproduced by theory[18] since

TABLE I. Frequencies (in meV) of some of the characteristic layer modes at the origin and zone boundaries of the surface Brillouin zone (experiment B).

Mode	Surface BZ symmetry point	3 ML	4 ML	5 ML	50 ML
α_1	$\bar{\Gamma}$	0.0	0.0	0.0	0.0
	$\bar{M}$	4.3	4.3	4.0	4.0
σ_1	$\bar{\Gamma}$				
	$\bar{M}$	6.0	6.0	6.0	5.9
ρ_1	$\bar{\Gamma}$			4.2	
	$\bar{M}$				
ε_1	$\bar{\Gamma}$	8.6	8.6	8.6	
	$\bar{M}$				
ε_2	$\bar{\Gamma}$		9.2	9.3	9.0
	$\bar{M}$				
α_2	$\bar{\Gamma}$				0.0
	$\bar{K}$				5.4
β_1	$\bar{\Gamma}$				
	$\bar{K}$	5.6	5.6	5.1	
δ_1	$\bar{\Gamma}$				
	$\bar{K}$	8.2		8.0	8.0
γ_1	$\bar{\Gamma}$	2.1		4.1	
	$\bar{K}$				
ε_1	$\bar{\Gamma}$	8.6	8.6	8.8	
	$\bar{K}$				
ε_2	$\bar{\Gamma}$		9.1	9.4	9.0
	$\bar{K}$				

its effect on the *effective* top layer spacing for the 4 ML film was found to be −8% compared to the bulk layer spacing, whereas for the 5 ML film it is +15% and larger than in the bulk. With increasing thickness, the effective top layer spacing converges toward the bulk value. More likely the effect reflects a stiffening of the radial force constant $\beta_\perp$ between the top and second layers, as predicted from the Rayleigh theorem.[58] Such a stiffening is consistent with the relaxation of the first layer, which has been measured by LEED for the bulk Pb(111) surface to be $-3.5\pm1.0\%$[59] and also for thin lead films (5–9 ML) on Si(111), −3%,[60] and −5%,[61] in reasonable agreement with the calculated relaxation for free-standing and Cu(111) supported lead films of about −6% (Ref. 18) and −7%,[22] respectively.

Recent first-principles calculations of the zone-center phonons for Pb(111) films with up to 14 layers also reveal the existence of one localized surface phonon slightly above the maximum bulk frequency, with an energy oscillating with the thickness, in tune with the oscillating compression of the first-to-second layer spacing.[24] This calculation for zone-center modes however predicts a stiffer mode for 3 and 5 ML and a softer mode at 4 ML, whereas the experiment for the 3 ML film places the ε mode below the maximum bulk frequency. As discussed in Sec. III D 3, the data for unannealed samples show a more pronounced disagreement with the results of Ref. 24.

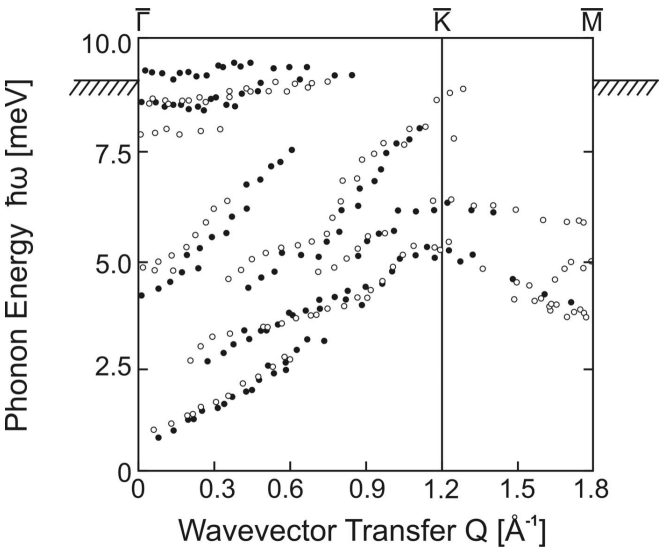

FIG. 10. Comparison of measured dispersion curves of a 5 ML film (experiment A) for freshly prepared (unannealed) surface (○) at $T_s=160$ K with measurements from the same film after annealing at 270 K and cooling back down to 160 K (●) along the $\bar{\Gamma}\bar{K}$ and $\bar{K}\bar{M}$ directions. The beam energy was $E_i=22$ meV.

Table I provides a summary of the experimental phonon frequencies at the origin and zone boundaries of the surface Brillonin zone. In contrast to the theory,[24] none of the mode frequencies show a significant dependence on the layer thickness.

3. Effects of annealing

Surface phonon dispersion curves were also measured (experiment A) for films freshly deposited at 140 K, which subsequently were not annealed. After annealing, the intensity of the diffuse elastic peak in the energy-transfer spectra was reduced by about 50%, indicating that the concentration of surface defects had also decreased by about the same amount. The biggest effect of annealing was an overall increase in the inelastic peak intensities. Otherwise, the time-of-flight and energy-transfer spectra appeared to be very similar. The results on the unannealed surfaces could be of some interest since the distortion and stress within the layers[61] should be much less.

Figure 10 compares the measured dispersion curves before and after annealing of a 5 ML film. The majority of the modes, which lie below about 7.5 meV are shifted downward, whereas the two branches of the $(\varepsilon_1,\varepsilon_2)$ doublet around 9 meV are increased by about 0.8 meV. This may be qualitatively understood in terms of a simple nearest-neighbor (nn) interaction potential $\varphi(r)$. The $(\varepsilon_1,\varepsilon_2)$ doublet and the (ρ_1,γ_1) pair at $\mathbf{Q}=0$ can be approximately associated with rigid displacements of the surface layer of SV and longitudinal polarization, respectively. In a nn force-constant model with the fcc structure, the interlayer force constants corresponding to these modes are, respectively, $\varphi_\perp=2\varphi''+\varphi'/r$ and $\varphi_\parallel=(\varphi''+5\varphi')/2$, where φ' and φ'' are the first

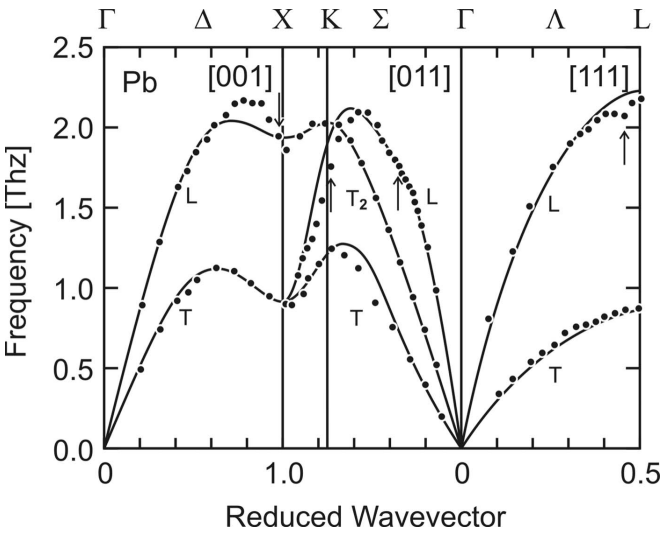

FIG. 11. Comparison of a best fit six nearest-neighbor force-constant calculation based on the parameters in Table II with neutron data of Brockhouse *et al.*[2] The vertical arrows mark Kohn anomalies which have been identified as such in the literature (Ref. 65).

and second derivatives of $\varphi(r)$. The variations $\Delta\varphi_{\perp}$ and $\Delta\varphi_{\parallel}$ produced by the annealing in the 5 ML film are proportional to the changes in the respective squared frequencies $\Delta[\hbar\omega(\varepsilon_1)]^2=11.4$ meV^2 and $\Delta[\hbar\omega(\gamma)]^2=-6.2$ meV^2 (see Fig. 10). In order to account for these variations, the nn radial and shear force constants have to change—relative to φ''—by the amounts $\Delta\varphi''/\varphi''\cong+18\%$ and $\Delta\varphi'/r\varphi''\cong-9.4\%$, respectively. Thus the annealing and the resulting adjustment of the atomic positions into a more compact configuration have the two-fold effect of stiffening the first interlayer radial force constant and of reducing the surface stress associated with the surface shear force constant φ'/r. Moreover, it gives an idea of the actual change in force constants in the surface bilayer with respect to the bulk force constants. As shown in Sec. IV A 2, a stiffening as large as ~30% of the nn radial force constants between atom pairs in the first two surface planes is required to qualitatively account for the observed dispersion curves in the annealed samples. It is natural to associate such a large stiffening of the force constants between first and second layers to a contraction of the first interlayer distance d_{12} as large as the value of −7% predicted by Jia *et al.*[22]

The effect of annealing thin lead layers on Cu(111) has also been studied with photoelectron spectroscopy.[62] Temperatures similar to those of the present study were used during growth: 100 K vs our 140 K and annealing at 300 K vs our 270 K. A number of different film thicknesses was initially present on the surface. Annealing had the effect of reorganizing the distribution of film heights favoring film heights with 6, 8, 10, 11, 15, and 17 ML similar to those observed by Otero *et al.*[16] Since the layer thickness in our experiment is well defined, such changes are not expected in the present experiment.

TABLE II. Best fit force constants of the bulk phonon dispersion curves measured by neutron scattering. β_n and α_n are the radial and tangential force constants between the nth neighbor atoms, respectively. All values are in N/m.

n	1	2	3	4	5	6
β_n	8.75	1.74	−0.61	1.91	−0.15	0.80
α_n	−0.61	−0.14	−0.28	0.19	−0.08	0.12

IV. DISCUSSION

A. Comparisons with Born–von Kármán fits

1. Bulk phonons

In an initial attempt to understand the dispersion curves, a six nn force-constant model calculation was carried out. This model was found to reproduce the bulk phonon dispersion curves to about the same extent as the earlier eight nn force-constant calculation of Cowley.[3] Figure 11 shows the fit obtained with the radial (β_n) and tangential (α_n) force constants tabulated in Table II.[63] If the interatomic force constants can be derived from a single interatomic potential $\varphi(r)$, then—as usual—$\beta_n\equiv\varphi''(r_n)$, $\alpha_n\equiv\varphi'(r_n)/r_n$ with r_n the distance between nth neighbors. In comparison with Cowley's fit, the new fit provides a better reproduction of the minimum in the L mode near the X point. As expected the force-constant model cannot fit the sharp dip in the L mode near the L point, which is due to a Kohn anomaly. Also the best fit curves lie above the data points for the L and T modes along the $\bar{\Gamma}\bar{X}$ direction, which again is in the region where Kohn anomalies affect the dispersion curves. The overall agreement is however comparable to that achieved with more sophisticated theories such as density-functional calculations.[5,6,8] Clearly in systems such as Pb films with important Fermi-surface effects such as Kohn anomalies, a Born–von Kármán force-constant analysis cannot tell anything about these effects but can nevertheless provide useful information about the interatomic forces which play a prominent role in the dispersion of each normal mode.

2. Surface phonons of 50 ML bulklike films

The force constants of Table II were then used in a slab calculation for a film on top of a rigid substrate. Surface equilibration is simply obtained by setting to zero the tangential force constants linking each atom of the top and bottom surface layers to the other atoms within the same layer. As anticipated earlier (Sec. III D 3), the fitting of the experimental upper branches requires a 30% stiffening of the radial force constant between the surface atoms and their nearest neighbors in the second layer. This surface model though neglecting surface stress[64] provides a sufficient basis for a qualitative discussion, especially for $Q\rightarrow 0$ at small wave vectors.

With respect to the interface with the substrate, an important advantage of using a Cu(111) substrate derives from the large mismatch in the frequencies of the light and stiff substrate and the heavy but soft lead layers. The effect of the coupling of the $\bar{\Gamma}$-point phonons with the substrate was in-

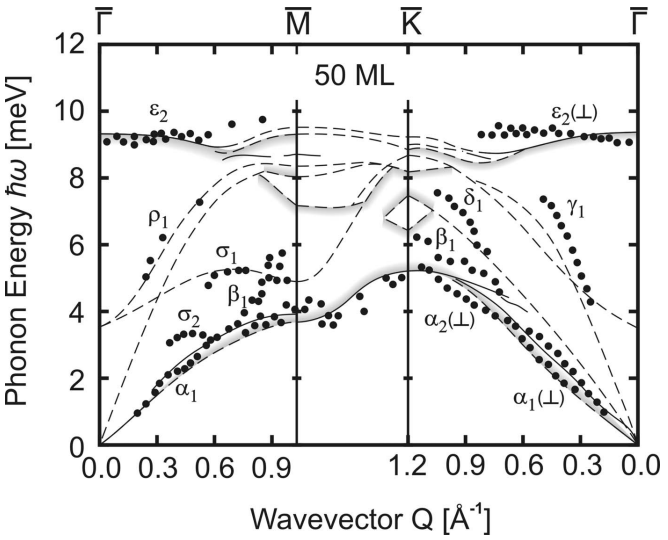

FIG. 12. Comparison between the measured surface phonon dispersion curves for a thick 50 ML Pb film with calculations based on the Born–von Kármán force constants in Table I.

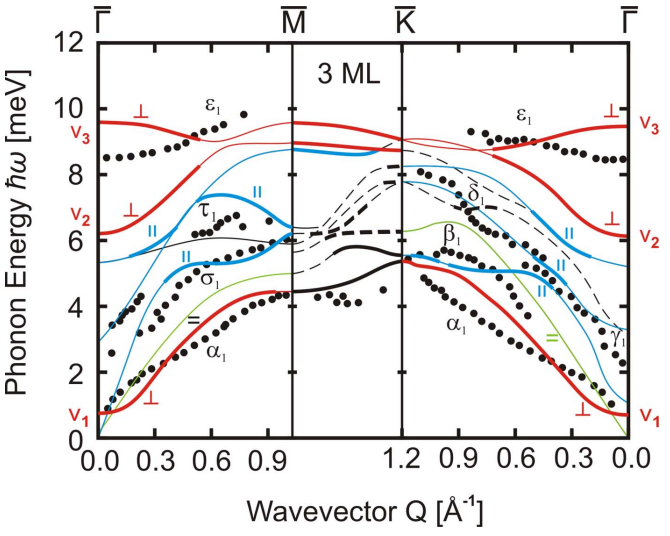

FIG. 13. (Color online) Comparison of calculated with experimental dispersion curves for a 3 ML film. The curves denoted by ⊥ are shear-vertical polarized near the $\bar{\Gamma}$ point. The modes labeled ∥ are longitudinally polarized and modes with = are shear horizontal. The heavy solid lines denote those parts of the dispersion curves with a large shear-vertical atomic displacement, which are expected to exhibit a large inelastic signal. The dashed lines mark modes, with unassigned polarizations. v_1, v_2 and v_3 label the predicted organ-pipe modes (Ref. 55).

vestigated by Luo *et al.*[55] From the observed decrease with layer thickness of the $\bar{\Gamma}$-point frequency of the lowest shear-vertical mode, the ratio of the film-substrate force constant β_f and the nn film force constant β_1 was estimated to be $\beta_f/\beta_1=1.14$.[55] The acoustic mismatch δ and the interface reflection coefficient R for lead films on Cu(111) were calculated to be 42.2% and 0.27, respectively, which indicate some coupling with the substrate.[55] On the other hand, in such cases of strong-coupling linear-chain simulations of the $\bar{\Gamma}$-point frequencies predict a large broadening of the film eigenmodes. The fact that this was not observed here provides some justification for the assumption made that the substrate is effectively rigid.

An alternative modeling of a weak film-substrate coupling is that of the quasi-free-standing film, where the interlayer force constants are symmetrical with respect to the film mirror plane (in the present case $\beta_1^{N,N-1}=\beta_1^{1,2}=1.3\beta_1$ and $\alpha_n^{1j}=\alpha_n^{Nj}=0$ for all n and $j=1,2,\ldots,N$) and only a very weak force constant β_f couples the bottom Nth layer to the substrate. In this model, $\beta_f/\beta_1=0.14$ is much smaller than predicted (see above) but is seen to provide a good fit of the experimental *RW* dispersion curves of the films. Actually the free-standing film model is seen to work well in the calculation of the electronic structure and the electronic quantum-size effects.[19] Since the interatomic force constants are essentially mediated by the conduction electrons, the quasi-free-standing film model is preferred in the present discussion.

Figure 12 presents a comparison between the measured surface phonon dispersion curves for a 50 ML film and calculations for the bulk surface based on the best fit force constants of Table II. Before interpreting the 50 ML data and the results for the thin films, we caution that a straight forward interpretation in terms of a force-constant model may lead to erroneous conclusions. There is now considerable evidence that the inelastic HAS signals on some metal surfaces are more strongly excited by the surface charge-density (SCD) oscillations induced by atom displacements than by the atomic displacements themselves. As recently shown for Cu(111),[26] larger SCD oscillations may be activated by subsurface modes, so that the association of the experimental dispersion curves with modes having a large amplitude at the surface may not always be justified. Nevertheless, since these effects require a lengthy sophisticated calculation the present results are interpreted simply in terms of the atomic amplitudes.

Along the $\bar{\Gamma}\bar{M}$ direction, the following modes can be identified. The mode labeled α_1 is obviously the Rayleigh mode (S_1). Though the energy is in fair agreement with experiment, in the calculation the mode is embedded in the bulk continuum and consequently should have only a weak signal. The experimental peak is, however, strong indicating a discrepancy with the expectation of the continuum theory, which is probably due to the oversimplified model. The modes designated β_1 and σ_2 are not clearly identifiable. σ_1 coincides with the upper edge of the shear-vertical bulk bands, while ρ_1 coincides with the upper edge of the longitudinal polarized bulk bands. Finally the ε_2 mode coincides nicely with the upper edge of the vertically polarized bulk bands, in agreement with experiment. This is a clear effect of the 30% stiffening of the surface radial force constant and is in contrast to the usual softening found for other metal surfaces or virtually no change as in the other simple metal Al.[66]

The observed modes along $\bar{\Gamma}\bar{K}$ are not so easily identified. The splitting of the Rayleigh mode to yield the modes α_1 and α_2 has not been observed previously in any system. The β_1 mode appears to be a resonance since it is embedded in the shear-vertical bulk bands. Its polarization is not clearly iden-

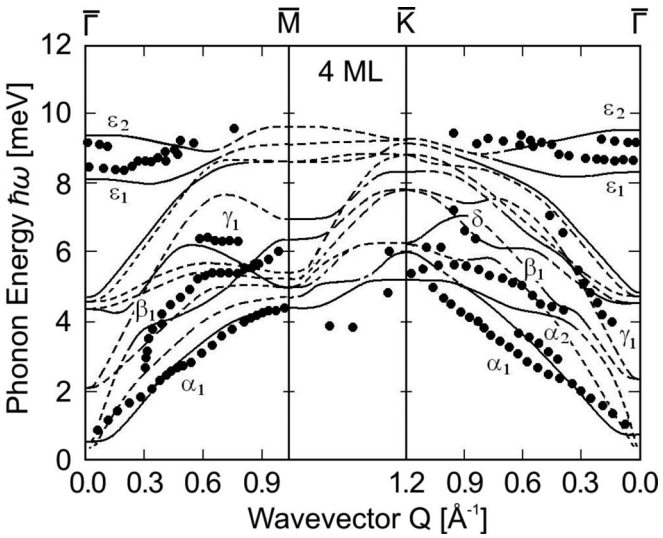

FIG. 14. Comparison of calculated with experimental dispersion curves for a 4 ML film. The heavy solid lines denote those parts with a large shear-vertical component. The dashed lines mark weaker parts or unassigned modes.

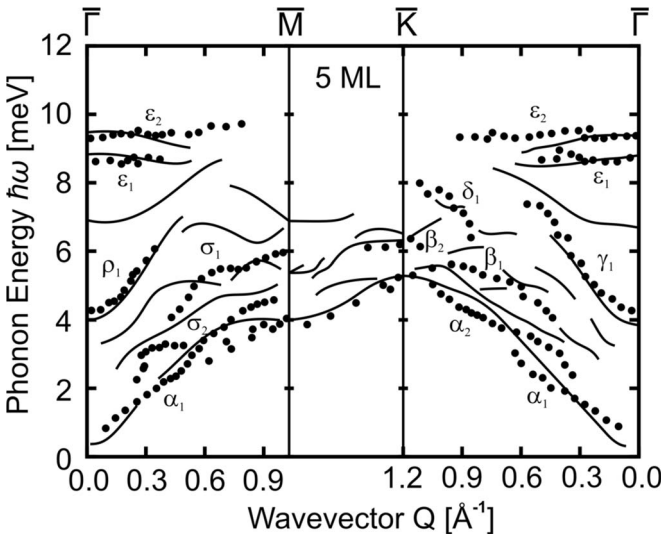

FIG. 15. Comparison of calculated with experimental dispersion curves for a 5 ML film. The heavy solid lines denote those parts with a large shear-vertical component.

tified in Fig. 5(d). δ_1 is also not easy to assign since it must be a sagittally polarized mode, even though it lies closest to what appears to be the bottom edge of a shear-horizontal band. γ_1 on the other hand lies close to the expected location of the longitudinally polarized bulk bands. ε_2 is a continuation of the same mode along $\bar{\Gamma}\bar{M}$ into the $\bar{\Gamma}\bar{K}$ direction.

The $\bar{\Gamma}\bar{K}$ direction is special since it has the same atomic arrangement as the bulk ΓK direction which has several Kohn anomalies (Fig. 11). Thus, some of the apparent anomalous behavior may be related to Kohn anomalies as discussed in Sec. IV B.

3. Phonons of 3, 4, and 5 ML films

Figure 13 shows a comparison of the calculated dispersion curves with the experimental data for 3 ML. The regions of the calculated curves with large shear-vertical components and corresponding large inelastic signals are indicated by the heavy continuous curves. The polarizations of the dashed line curves have not been assigned.

Along the $\bar{\Gamma}\bar{M}$ direction, the α_1 mode is slightly softened at intermediate wave vectors. The σ_1 mode seems to lie in the general region of the lowest longitudinal mode. At about 0.6 $Å^{-1}$, it crosses the predicted curve and at larger wavelengths lies above the theoretical curve. The τ_1 mode is below the nearest vertically polarized mode. The highest vertically polarized mode ε_1 deviates significantly from the predicted shape.

Along $\bar{\Gamma}\bar{K}$ the assignment is even more difficult because of the greater congestion. The α_1 mode is softened even more than in the $\bar{\Gamma}\bar{M}$ direction. The γ_1 and β_1 modes can be assigned to the nearby longitudinal mode or could even be due to an extreme softening of the next-higher predicted longitudinal mode, which starts at about 5.3 meV. Again the ε_1 mode is greatly distorted compared to the predicted shape.

The comparison between theoretical and experimental phonons for the 4 ML film is shown in Fig. 14. The 4 ML film is, as mentioned earlier, particularly interesting because of the apparent contraction in the effective distance between the two top most layers, which is interpreted as due to a reduced electron spillout of the fourth layer.[15,18] The assignment of the observed modes is even more difficult than for the 3 ML film. Along the $\bar{\Gamma}\bar{M}$ direction a α_1 mode—is as for the 3 ML film—softened at intermediate wave vectors. The σ_1 mode could be attributed to a softening of the above lying shear-vertical polarized "hump" mode or a distortion of the vertically polarized mode which it straddles. Most interesting is the much improved agreement between theory and experiment of the ε_1 and ε_2 modes. The situation along $\bar{\Gamma}\bar{K}$ is as in the other films more complicated. Particularly noteworthy is the large softening of the α_1 Rayleigh mode and the appearance of another α_2 mode directly above. The latter cannot be a softened part of the above-lying longitudinal branch since it has a large vertical component as indicated by Fig. 5(b). As in the $\bar{\Gamma}\bar{M}$ direction, the ε_1 and ε_2 modes agree rather well with theory.

The 5 ML film dispersion curves (Fig. 15) also show some elements of agreement and other regions where the relation to the theory is not obvious. Along $\bar{\Gamma}\bar{M}$ the lowest α_1 mode appears to be split. The lower branch ending at 4 meV at $\bar{M}$ was only found in experiment A and thus is uncertain. It is shown here since it fits nicely with the data points between $\bar{M}$ and $\bar{K}$. Neither the σ_1 nor the σ_2 mode can be easily assigned. On the other hand, ρ_1 is obviously the upper edge of the shear-vertical bulk band. The $(\varepsilon_1,\varepsilon_2)$ doublet is again well reproduced. Along $\bar{\Gamma}\bar{K}$ the apparent splitting of the Rayleigh mode, which was seen to a lesser extent for 4 ML, is well developed and is also seen for the thick 50 ML film (Figs. 9 and 12). Like ρ_1 along $\bar{\Gamma}\bar{M}$, γ_1 marks the top of the shear-vertical bulk band.

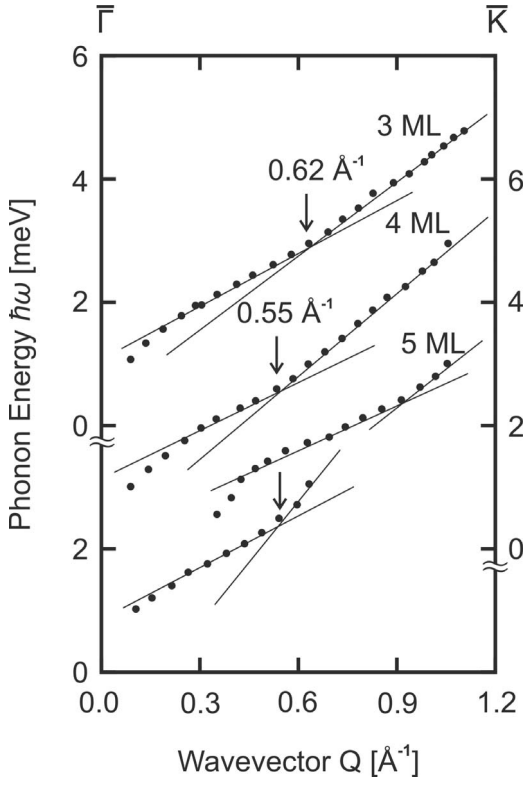

FIG. 16. Straight line fits to the data points of the lowest dispersion curves along the $\bar{\Gamma}\bar{K}$ direction for the 3, 4, and 5 ML films are used to identify possible Kohn anomalies indicated by vertical arrows. The splitting in the 5 ML dispersion complicates the assignment and one of several possible interpretations is suggested.

B. Evidence for Kohn anomalies.

As mentioned in Sec. I Kohn anomalies have only been observed on a few clean metal surfaces, namely, Pt(111),[29] H/W(110),[30] and H/Mo(001).[31] In the case of Pt(111), two Kohn anomalies could be identified on the basis of small dips in the Rayleigh mode dispersion curve along the $\bar{\Gamma}\bar{K}$ direction. This surface direction has the same atomic arrangement as the $\bar{\Gamma}\bar{K}$ bulk direction for which an anomaly had also been reported for the bulk transverse T_1 mode.[2] Since in the Pb films the Rayleigh modes appear over a broad range of wave vectors and are relatively well isolated from other modes, they are a logical place in which to look for similar anomalies. Figure 16 shows an enlarged view of the measured dispersion curves of the lowest mode in the $\bar{\Gamma}\bar{K}$ direction in the 3, 4, and 5 ML films. To determine the location of the anomalies, straight lines have been fitted to the far right and far left regions of the dispersion curves. The wave vector at which these straight lines cross mark the locations of the anomalies. The interpretation appears to be quite straightforward for the anomalies at 0.62 and 0.55 Å^{-1} for the 3 and 4 ML films but is not all clear in the case of the 5 ML film for which the measurements indicate a splitting of the dispersion curves at about the same wave vector as the kink in the 3 and 4 ML films. The possible location of an anomaly is indicated by the arrow placed at about Q =0.55 Å. Surprisingly, the locations for all three films are in very good agreement with the bulk anomaly which is at 0.57 Å^{-1}.[65]

V. SUMMARY

Thin atomically smooth films of Pb (111) with well-defined thicknesses of N=3, 4, and 5 MLs and a thick bulk-like 50 ML film have been grown on the Cu(111) surface and characterized with inelastic helium atom scattering. The diffraction patterns reveal the expected (111) structure with the same lattice parameters as the bulk surface and a small effect of the $p(4\times4)$ structure of the first layer. The time-of-flight spectra show a rich structure. The dispersion curves exhibit more than half of the maximum $2N$ number of dispersion curves with vertical and longitudinal (sagittal plane) polarizations, which can be excited along the high-symmetry directions. The number of phonons observed is larger than found in all other previous thin-film investigations. Since, moreover, most of these modes pervade throughout the entire film slab with amplitudes which are not necessarily localized at the surface, it appears that the helium atoms are remarkably sensitive to the phonons of these lead films. A notable exception is represented by the mode ε_2 which occurs above the maximum bulk frequency at all thicknesses and is therefore localized at the surface. This mode results from the strong contraction of the first interlayer spacing. It remains for future theories to establish if this remarkable sensitivity is another case in which the surface charge densities induced by atomic displacements within the slab account for a strong coupling of the He atoms also to subsurface modes as recently demonstrated for the Cu(111) surface.[26] Along the [110] direction, a surface Kohn anomaly is identified at about the same wave vector of 0.54 Å found along the equivalent direction in the bulk.

The experimental curves are compared with calculated dispersion curves based on Born–von Kármán force constants which have been fitted to the bulk force constants and modified to avoid surface instabilities. The agreement is in most cases only qualitative. This is perhaps not surprising in view of the inability of the force-constant model to reproduce all the bulk phonon features dependent on Fermi-surface effects, especially the Kohn anomalies. Since these anomalies become more distinct with reduced dimensionality,[28] the effect of this inadequacy is expected to be amplified in the thin films. In addition, in making the comparison the following additional approximations are introduced. (1) The dynamic coupling to the Cu substrate is neglected as discussed in Sec. IV A 2. (2) The perturbation of the electronic bands of the lead surface by the Cu bands is neglected. Since, however, the Cu bulk bands only affect the low-lying Pb levels at about 5 eV below the vacuum level,[20,21] the effect on the bonding electrons on the lead layers is not expected to be significant. (3) The Pb films are assumed to have an ideal (111) structure throughout. In previous studies, the monolayer has been shown to have a $p(4\times4)$ structure which results from the large mismatch between the Pb bulk lattice constant (a=4.95 Å) and the Cu lattice constant (a=3.61 Å). The present results indicate that this structure also affects to a lesser extent the other layers.

Perhaps more serious in this context are possible effects coming from the second layer for which we are not aware of any information on its structure. Some ideas as to what might be expected comes from LEED studies during growth of an additional 0.2 ML on top of 1 ML film at 180 K, which indicates a 3.3% increased compression.[43] After annealing to 800 K, the compression disappeared and the lattice constant was only slightly greater than in the bulk. The HAS angular distributions indicate no significant compression (within less than 2%) either for the unannealed nor for the annealed film surfaces.[47] Finally (4) the Cu substrate was assumed to be unaffected by the lead overlayer. A recent combined LEED, scanning tunnel microscope (STM), and Auger studies revealed a complex restructuring of the first three layers of the Cu substrate,[67] which will further complicate the structure at the interface.

Obviously this interesting thin-film system which has already attracted a very large number of experimental and theoretical investigations still holds formidable challenges for the theory. Hopefully it will soon be possible to fully simulate the bulk Kohn anomalies and then tackle the problem of calculating the phonon dispersion curves for the thin supported films. Some encouraging results in this direction have already been achieved.[27]

ACKNOWLEDGMENTS

We wish to especially thank Ningsheng Luo for his assistance in carrying out the Born von Kármán force constant calculations. We are also very grateful to Peter Saalfrank (University of Potsdam), Johannes Pollmann (University of Münster), as well as to Evgueni Chulkov, P. M. Echinique, and Irina Sklyadneva [Donostia International Physics Center (DIPC), San Sebastian, Spain] for enlightening discussions and correspondence. We thank Erio Tosatti (Trieste, SISSA/ICTP) for calling our attention to the recent article by Dal Corso. One of us (G.B.) acknowledges the support of the Alexander von Humboldt Foundation for visits to Göttingen and of the DIPC during the early and final stages of this study, respectively.

*Present address: Qimonda AG, Gustav-Heinemann-Ring 212, 81729 Munich, Germany.
†Present address: Department of Physics, Universitá degli Studi di Cagliari, I-09042 Monseratto (CA), Italy
‡Present address: SAP AG, Dietmar-Hopp-Allee 16, 69190 Walldorf, Germany.
§Corresponding author; jtoenni@gwdg.de

[1] G. Grimvall, *The Electron-Phonon Interaction in Metals* (North-Holland, Amsterdam, 1981).
[2] B. N. Brockhouse, T. Arase, G. Caglioti, K. R. Rao, and A. D. B. Woods, Phys. Rev. **128**, 1099 (1962).
[3] E. R. Cowley, Solid State Commun. **14**, 587 (1974).
[4] X. M. Chen and A. W. Overhauser, Phys. Rev. B **39**, 10570 (1989).
[5] S. de Gironcoli, Phys. Rev. B **51**, 6773 (1995).
[6] S. Y. Savrasov and D. Y. Savrasov, Phys. Rev. B **54**, 16487 (1996).
[7] B. Grabowski, T. Hickel, and J. Neugebauer, Phys. Rev. B **76**, 024309 (2007).
[8] A. Y. Liu and A. A. Quong, Phys. Rev. B **53**, R7575 (1996).
[9] A. Dal Corso, J. Phys.: Condens. Matter **20**, 445202 (2008).
[10] B. J. Hinch, C. Koziol, J. P. Toennies, and G. Zhang, Europhys. Lett. **10**, 341 (1989).
[11] M. Jałochowski, H. Knoppe, G. Lilienkamp, and E. Bauer, Phys. Rev. B **46**, 4693 (1992).
[12] M. Jałochowski, M. Hoffmann, and E. Bauer, Phys. Rev. Lett. **76**, 4227 (1996).
[13] Y. Guo, Y.-F. Zhang, X.-Y. Bao, T.-Z. Han, Z. Tang, Li-X. Zahng, W.-G. Zhu, E. G. Wang, Q. Niu, Z. Q. Qiu, J.-F. Jia, Z.-X. Zaho, and Q.-K. Xue, Science **306**, 1915 (2004).
[14] P. S. Kirchmann, M. Wolf, J. H. Dil, K. Horn, and U. Bovensiepen, Phys. Rev. B **76**, 075406 (2007).
[15] J. Braun, Ph.D. Dissertation, University of Göttingen, 1997; Max-Planck-Institut für Strömungsforschung Report No. 11, 1997 (unpublished).
[16] R. Otero, A. L. Vázquez de Parga, and R. Miranda, Phys. Rev. B **66**, 115401 (2002).
[17] P. Saalfrank, Surf. Sci. **274**, 449 (1992).
[18] G. Materzanini, P. Saalfrank, and P. J. D. Lindan, Phys. Rev. B **63**, 235405 (2001).
[19] C. M. Wei and M. Y. Chou, Phys. Rev. B **66**, 233408 (2002).
[20] E. Ogando, N. Zabala, E. V. Chulkov, and M. J. Puska, Phys. Rev. B **69**, 153410 (2004).
[21] E. Ogando, N. Zabala, E. V. Chulkov, and M. J. Puska, Phys. Rev. B **71**, 205401 (2005).
[22] Y. Jia, B. Wu, H. H. Weitering, and Z. Zhang, Phys. Rev. B **74**, 035433 (2006).
[23] A. Ayuela, E. Ogando, and N. Zabala, Phys. Rev. B **75**, 153403 (2007); Appl. Surf. Sci. **254**, 29 (2007).
[24] F. Yndurain and M. P. Jigato, Phys. Rev. Lett. **100**, 205501 (2008).
[25] J. Braun and J. P. Toennies, Surf. Sci. **384**, L858 (1997).
[26] V. Chis, B. Hellsing, G. Benedek, M. Bernasconi, E. V. Chulkov, and J. P. Toennies, Phys. Rev. Lett. **101**, 206102 (2008).
[27] E. V. Chulkov and I. Sklyadneva (private communication).
[28] E. Tosatti, in *Festkorperprobleme*, Advances in Solid State Physics, edited by H. J. Queisser (Vieweg, Braunschweig, 1975), Vol. 15, p. 113; P. Ziesche and G. Lehmann, *Ergebnisse in der Elektronentheorie der Metalle* (Akademie, Berlin, 1983), p. 343.
[29] U. Harten, J. P. Toennies, C. Wöll, and G. Zhang, Phys. Rev. Lett. **55**, 2308 (1985).
[30] E. Hulpke and J. Lüdecke, Phys. Rev. Lett. **68**, 2846 (1992).
[31] E. Hulpke and J. Lüdecke, Surf. Sci. **287-288**, 837 (1993).
[32] M. Balden, S. Lehwald, and H. Ibach, Phys. Rev. B **53**, 7479 (1996).
[33] G. Benedek, G. Brusdeylins, C. Heimlich, L. Miglio, J. G. Skofronick, J. P. Toennies, and R. Vollmer, Phys. Rev. Lett. **60**, 1037 (1988); G. Brusdeylins, C. Heimlich, J. G. Skofronick, J. P. Toennies, R. Vollmer, G. Benedek, and L. Miglio, Phys. Rev. B **41**, 5707 (1990).

[34] G. W. Witte, Ph.D. Dissertation, University of Göttingen, 1995; Max-Planck-Institut für Strömungsforschung Report No. 8, 1995 (unpublished).
[35] G. Benedek, J. Ellis, A. Reichmuth, P. Ruggerone, H. Schief, and J. P. Toennies, Phys. Rev. Lett **69**, 2951 (1992).
[36] E. Hulpke, J. Lower, and A. Reichmuth, Phys. Rev. B **53**, 13901 (1996).
[37] J. D. White, J. Cui, M. Strauss, R. D. Diehl, F. Ancilotto, and F. Toigo, Surf. Sci. **307-309**, 1134 (1994).
[38] J. Braun and J. P. Toennies, Surf. Sci. **368**, 226 (1996).
[39] G. Lilienkamp and J. P. Toennies, J. Chem. Phys. **78**, 5210 (1983).
[40] B. J. Hinch, A. Lock, H. H. Madden, J. P. Toennies, and G. Witte, Phys. Rev. B **42**, 1547 (1990).
[41] J. P. Toennies and K. Winkelmann, J. Chem. Phys. **66**, 3965 (1977).
[42] The temperatures used for annealing were somewhat lower than those recommended in Ref. 40 since desorption was found at $T \geq 270$ *K*.
[43] G. Meyer, M. Michailov, and M. Henzler, Surf. Sci. **202**, 125 (1988).
[44] C. Nagl, O. Haller, E. Platzgummer, M. Schmid, and P. Varga, Surf. Sci. **321**, 237 (1994).
[45] G. Drolshagen, A. Kaufhold, and J. P. Toennies, Isr. J. Chem. **22**, 283 (1982).
[46] L. J. Gómez, S. Bourgeal, J. Ibáez, and M. Salmerón, Phys. Rev. B **31**, 2551 (1985).
[47] G. Zhang, Ph.D. Dissertation, University of Göttingen, 1990; Max-Planck-Institut für Strömungsforschung Report No. 102, 1991 (unpublished).
[48] See footnote 56 in Ref. 51.
[49] D. Farias and K.-H. Rieder, Rep. Prog. Phys. **61**, 1575 (1998).
[50] The corrugation of a thick ($\geq$50 ML) Pb(111) film was determined using an eikonal analysis of the He atom diffraction intensities based on the following rigid surface corrugation function assuming a well depth of 7 meV: $\varsigma(\vec{R}) = 2\varsigma_1^{(2)}\{\cos(G_2 x) + \cos[G_2(\frac{x}{2} + \frac{\sqrt{3}}{2}y)] + \cos[G_2(\frac{x}{2} + \frac{\sqrt{3}}{2}y)]\} + 2\varsigma^{(0)}\{\cos[G_0(\frac{\sqrt{3}}{2}x - \frac{y}{2})] + \cos[G_0(\frac{\sqrt{3}}{2}x + \frac{y}{2})] + \cos(G_0 y)\}$ where G_0 is the lattice vector along the (110) azimuthal direction and G_2 is the lattice vector along the (112) azimuthal direction. $\varsigma_1^{(2)}$ is the first-order corrugation amplitude along the (112) direction and $\varsigma^{(0)}$ is the first-order corrugation amplitude along the (110) direction. At an incident-beam energy of 22 meV, $\xi_1^{(2)} = 0.012 \pm 0.001$ Å und $\xi_1^{(0)} = 0.000\,4 \pm 0.000\,1$ Å (Ref. 44).
[51] D. M. Smilgies and J. P. Toennies, Rev. Sci. Instrum. **59**, 2185 (1988).
[52] R. B. Doak in *Atomic and Molecular Beam Methods*, edited by G. Scoles (Oxford University Press, New York, 1992), Vol. 2, p. 384.
[53] D. Eichenauer, H. Harten, J. P. Toennies, and V. Celli, J. Chem. Phys. **86**, 3693 (1987).
[54] C. Kaden, P. Ruggerone, J. P. Toennies, G. Zhang, and G. Benedek, Phys. Rev. B **46**, 13509 (1992).
[55] N. S. Luo, P. Ruggerone, and J. P. Toennies, Phys. Rev. B **54**, 5051 (1996).
[56] V. Bortolani and G. Santoro, Surf. Sci. **148**, 82 (1984).
[57] G. W. Farnell, in *Physical Acoustics*, edited by W. P. Mason and R. N. Thurston (Academic Press, New York, 1970/Springer-Verlag, Berlin, Heidelberg, 1978), Vol. 6, p. 109.
[58] A. A. Maradudin, P. Mazur, E. W. Montroll, and G. H. Weiss, Rev. Mod. Phys. **30**, 175 (1958).
[59] Y. S. Li, F. Jona, and P. M. Marcus, Phys. Rev. B **43**, 6337 (1991).
[60] A. Mans, J. H. Dil, A. R. H. F. Ettema, and H. H. Weitering, Phys. Rev. B **72**, 155442 (2005).
[61] P. Czoschke, H. Hong, L. Basile, and T.-C. Chiang, Phys. Rev. B **72**, 035305 (2005).
[62] J. H. Dil, J. W. Kim, S. Gokhale, M. Tallarida, and K. Horn, Phys. Rev. B **70**, 045405 (2004).
[63] N. S. Luo and P. Ruggerone (private communication).
[64] In a simple nearest-neighbor interaction model, the surface stress is given by $\tau = \alpha_1/2$, where α_1 is the interatomic tangential force constant in the surface layer; see R. Shuttelworth, Proc. Phys. Soc. London **A63**, 444 (1950).
[65] B. N. Brockhouse, K. R. Rao, and A. D. B. Woods, Phys. Rev. Lett. **7**, 93 (1961).
[66] A. Franchini, V. Bortolani, G. Santoro, V. Celli, A. G. Eguiluz, J. A. Gaspar, M. Gester, A. Lock, and J. P. Toennies, Phys. Rev. B **47**, 4691 (1993).
[67] S. Müller, J. E. Prieto, C. Rath, L. Hammer, R. Miranda, and K. Heinz, J. Phys.: Condens. Matter **13**, 1793 (2001).